Experimental study on transient frictional features of herringbone-grooved mechanical face seals in start-up and stop stages

Yongfan Li, Noël Brunetière, Muming Hao, Tianzhao Li, Fuyu Liu

Experimental study on transient frictional features of herringbone-grooved mechanical face seals in start-up and stop stages

Yongfan LI[a, b], Noël BRUNETIÈRE[b], Muming HAO[a *], Tianzhao LI[a], Fuyu LIU[a]

[a] Institute of Sealing Technology, College of New Energy, China University of Petroleum (East China), Qingdao 266580, Shandong, China

[b] Institut Pprime UPR 3346, CNRS - Université de Poitiers - ISAE ENSMA, Futuroscope Chasseneuil 86962, France

* Corresponding author. E-mail address: haomm@upc.edu.cn

Abstract: Evolutions of frictional features of herringbone-grooved face seals during start-up and stop stages are focused on. Transient frictional torques are measured for outer-diameter-side, middle and inner-diameter-side grooved seals and a smooth-face seal based on a formerly developed dedicated test rig. Development of fluid carrying capacity can be deduced for all four seals according to torque evolutions, and lift-off mechanisms are analyzed. Hydrodynamic effect gets smaller with grooves apart from pressurized fluid side, and thereby hydrostatic effect due to face coning by heat generation dominates the fluid film formation as it is for the smooth-face seal. Thermal characteristic time due to thermal lag effect is smaller than accelerating periods. The squeeze effect indicated by the smaller torque of stop stages is also playing a role in transient operation.

Keywords: mechanical face seals, lift-off mechanism, frictional torque, transient performance

1. Introduction

Mechanical face seals are essential basic components of the rotating fluid-delivery machinery [1]. Face modification technique has been all along implemented to improve the performance of face seals. The spiral groove and its derivative patterns such as the herringbone groove and other double-row grooves have been studied and even applied due to advantages of lubrication improvement and leakage inhibition [2][3][4][5][6][7]. Comparing with the typical spiral-grooved face seal, the herringbone-grooved seal tends to balance the conflict of long lifetime and low leakage much more efficiently [8][9].

Since Strom et al. [10] first explained the principle of the herringbone-grooved face seal which was utilized on the high-temperature liquid sodium sealing in the 1960s, this technique has been further developed in different patterns of double-row spiral grooves [8][11]. As a typical work, Wang et al. focused on the splayed spiral-grooved oil-film-lubricated face seal and carried out systematic work on theoretical analyses [12], experimental research and field applications [13]. In addition, a complex structure composed of both spiral and herringbone grooves was proposed by Zhang et al. [5][14], and the theoretical analyses and the transient and steady-state experiments were executed. Zheng et al. [15][16] [17] combined the herringbone grooves with the hydrostatic orifices through the face and applied it in high-speed, high-temperature and large-diameter gas engines. Meng et al. [9] proposed a quasi-3D thermal-hydrodynamic lubrication numerical model, and carried out a parametric analysis about the influence of the structural parameters of the herringbone grooves on the performance. Xu et al. [18] applied the herringbone groove structure to a new type of composite face seal that relies on superconducting magnetic force to improve lubrication effect and stability.

As for the experimental tests of other types of face seals, Chen et al. [19] conducted experimental tests on the frictional toque of a multi-scale composite textured face seal at different rotation speeds and medium pressures, obtaining a lower and more stable friction torque than the un-textured seal. Chang et al. [20] verified the friction factor fractal model of the end face by measuring frictional coefficient of a B104a-70 mechanical seal. The lubrication improvement and temperature reduction effects of the textured face seal comparing with the smooth-face seal were verified by measuring the face temperature with an infrared camera and the frictional torque with a dedicated mechanism under a certain range of rotation speed [21]. With the same test rig, Ayadi et al. [22][23] studied the lubrication regimes and the thermal features of a common mechanical seal separately with a force sensor and thermocouples. Xue et al. [24] regarded the vehicle wet clutches as the background to study the separation characteristics of the spiral

groove rotary face seals by experimentally and theoretically establish the frictional torque (also the frictional coefficient) - rotation speed relationship with the steady-state results, especially focusing on the influence of the groove structural parameters. Aiming at the same objective, Zhao et al. [25] built a novel test setup to measure the oil-film stiffness, verifying theoretical models; besides, the sealing characteristics were also involved [26]. Ma et al. [27] experimentally investigated the frictional properties of the radially varying-diameter-dimple face seals under normal pressure lubricant. Xu et al. [28] experimentally studied the wear behavior of the high-pressure side of the spiral groove dry gas seal. Ding et al. [29] utilized the Type PT100 sensors to measure the film temperature of a spiral groove dry gas seal at three radial positions. Feng et al. [30] measured the leakage of the waviness mechanical seals. A vertical visible test rig was used to comparatively study the hot water two-phase seals with and without laser face texturing, and the frictional torques were also measured at different rotation speed; a pulse at the starting can be observed from the curves of torque evolution, but this phenomenon was not the concern [31]. Similar test setup was adapted to investigate the tribological performance of laser textured stainless steel rings [32]. Li et al. [3] developed a set of internally pressured visible test assembly for the spiral groove oil-film face seal to observe the distribution and formation of the cavitation, and the influences of speed, oil pressure, groove depth and spiral groove are specifically analyzed. Chen et al. [33] carried out experimental studies on transient film thickness and leakage rate of a spiral groove dry gas seal at high-speeds under different spring pressures and different spiral groove depths to verify the perturbation method of dynamic analysis.

As investigated and summarized above, in addition to the leakage, the frictional features and the temperatures of the seal faces are the main concerns of experimental researches for the mechanical face seals. Besides, the visible observations and the dynamic properties of the fluid film for the hydrodynamic-lubrication seal type are also involved. As generally agreed, the frictional state could directly impact the heat generation and reflect the film-formation stability. Meanwhile, although the speed-varying operating conditions exist in applications, mostly these tests focus on the steady-state phenomena and performance.

The present work takes the herringbone-grooved face seals as the targets, and the frictional torque variations during the start-up and stop stages are measured. Developments of the lubrication state during the transient processes are compared and analyzed among three herringbone-grooved face seals and a smooth-face seal based on the frictional torque results.

2. Experimental apparatus and procedure

2.1. Test rig

The test rig utilized in the present work has been formerly introduced and adapted by Brunetiere et al. [6][21][22] on the steady-state performance of mechanical seals including the frictional torque. The general view of the test rig is illustrated in **Fig. 1(a)**, which is composed of the synchronous converter motor, the transmission shaft, the spindle housing and the experimental cell embedding on the front of it. To achieve the accurate direct measurement of the frictional torque of the seal face, the rotational degree-of-freedom is added to the experimental cell by setting a double-conical hybrid bearing contained in the spindle housing. Therefore, with the preload tensing the force sensor via a steel wire that is fixed onto the cell bottom, any additional torque driven by the rotor faces of the seals can be gathered by this force sensor. The front view of the test rig is shown in **Fig. 1(b)**.

2.2. Experimental cell and measurements

The cross-section structure of the experimental cell is presented in **Fig. 2(a)**. Two mechanical face seals with same structure and size are configurated in the front and back sides of chamber. The assembling spaces for both seals are also same so that the seals can operate in approximate identical environmental condition. Meanwhile, the back-to-back arrangement makes the axial unbalanced load from the pressured fluid onto the shaft removed. Pressured hot water from a piece of hydraulic circulating equipment goes through the cell from the bottom to the top. Thermocouples and a pressure sensor are mounted through the chamber for measuring the water temperature and pressure in it. The leakage dropping can be collected via two drain tubes and monitored by a high-precision electric balance. Due to the front-and-back configuration of two seals in the cell, both of the obtained frictional torque and leakage data are equivalent to results from twice tests. The technical parameters of the utilized sensors are listed in **Table 1** [6].

Table 1 Technique parameters of the sensors.

Sensors	Type	Accuracy	Range
force sensor	FN3148	≤ 0.05% of the range	500 N
thermocouples	T type	± 0.5 °C	350 °C
pressure sensor	XPMC10	± 0.01 MPa	5 MPa
electric balance	BJ6100d	± 0.1 g	6100 g

2.3. Monitor and control system

The monitor and control system of the whole experimental equipment is developed based on the NI hardware and the LabVIEW platform. Via the self-developed LabVIEW software:

(1) the temperature, pressure and flow rate of the water supply can be controlled and monitored;

(2) the starting up and stop of the motor can be controlled, and the rotation speed can be set and monitored;

(3) the torque from the experimental cell and the weight on the electric balance can be monitored;

(4) the temperature and pressure of the lubricant supply for the spindle housing can be monitored.

All of these data can be monitored and saved in real time. Therefore, the transient performance can be accurately measured even in very short duration.

2.4. Target seals

The structure of the target seal is shown in **Fig. 2(b)**. The stator is a transparent disk made of the sapphire material aiming at infrared thermal imaging of the rotor face but not concerned in this paper. The rotor is made of tungsten carbide with cobalt (WC-Co) that is not only softer than sapphire but also easy to machine the shallow grooves by laser. The inner and outer radii of the seal face are respectively 25.9 mm and 31.5 mm. The pressure of the spring force on the face is approximate 0.11 MPa, indicating a spring force of 111 N. With a designed balance ratio of 0.7, the medium force can be calculated as the medium pressure is given.

Totally four types of seal are tested. As shown in **Fig. 3**, three of them are grooved faces and the rest one is smooth-face. For each type, we have the front-side and back-side specimens. The herringbone-groove rows are machined by laser separately at the outer-diameter side, the middle and the inner-diameter side of the faces (named the outer-groove seal, the middle-groove seal and the inner-groove seal). As shown in **Fig. 4**, for one single herringbone groove, the geometry is controlled by the outer, middle and inner radii, as well as the spiral angle of the groove boundary. Therefore, the structural parameters of the rotor faces are summarized in **Table 2**.

Table 2 Structural parameters of the rotor faces.

	outer-groove seal	**middle-groove seal**	**inner-groove seal**	**smooth-face seal**
outer radius of face r_o / mm	31.5			
inner radius of face r_i / mm	25.9			
spiral angle α / °	20			-
groove number	24			-
groove depth h_g / μm (the WC-Co rotors)	15, roughness in grooves: $Sa < 0.8$ roughness on face: $Sa < 0.1$			-
groove-to-land width ratio	1:1			-
outer radius of groove r_{go} / mm	31.5	30.4	28.1	-
middle radius of groove r_{gm} / mm	30.4	29.3	27	-
inner radius of groove r_{gi} / mm	29.3	28.2	25.9	-

2.5. Experimental procedure

The process of the start-up stage is set as from 0 r/min to 3500 r/min versus the stop stage set as 3500 r/min to 0 r/min. The variation mode of the rotation speed is set as linear, but during the very first about 0.8 s and the last about 0.8 s the speed evolution would be non-linear due to the performance limitation of the motor driving system. Therefore, it could not be strictly linear speed rising or dropping processes.

Five speed-varying rates (the acceleration or the deceleration of the rotation speed variations) are selected to cover a relatively large range of start-up or stop conditions, which are 8 s/kr, 4 s/kr, 2 s/kr, 1 s/kr and 0.5 s/kr. Taking the non-linear stages into account, the transient durations of speed varying are correspondingly about 28 s, 15 s, 8 s, 4.5 s, 2.8 s.

The water temperature, pressure and flow rate are respectively selected as 60 °C, 0.5 MPa(G) and 30 L/min.

The transient frictional torque evolutions during the start-up and stop stages are the main concerns of the tests. The experimental procedure is described as:

(1) measurement of the torque reference at standstill: finish the assembly of the experimental cell and the water inlet and outlet pipes; disconnect the motor at the transmission shaft; start the oil supply for the spindle housing; start the water supply for the cell with the selected conditions; record the torque as the reference.

(2) running and measurement for one complete start-up and stop process: stop the oil supply and the

water supply, and connect the spindle with the motor; restart both supply systems; set the speed-varying rate on the motor controller; start the data saving on the software and start the motor; after it reaches 3500 r/min and runs for 1 ~ 2 min, stop the motor and finish the stop stage running.

(3) repeat the above steps for each condition, and finish all of 60 times of test.

3. Results

3.1. Original data of the frictional torque evolutions

The frictional torques are measured for the outer-groove, middle-groove, inner-groove and smooth-face seals during the start-up and stop stages at five speed-varying rates. To check the repeatability and the accuracy of the measurement, tests of all conditions are repeated three times. All of the torque evolution results of 120 tests are presented in **Fig. 5** ~ **Fig. 8**. In each sub-figure is the curves of the repeated tests.

A fundamental finding is that in all sub-figures three curves demonstrate good consistency in both tendency and value, indicating that the test method for the transient frictional torque is sufficiently accurate and reliable and that the results are in good repeatability.

The common features of the torque evolutions of the start-up stages with the speed rising can be summarized as: (1) the torques rapidly go to a peak point from a low value (zero or above zero), especially, it is found that the peaks occur at almost the same time (at about 1 s) not only for three repeated tests in each sub-figure, but also for all four seals and all five rates; (2) a clear descent stage follows the peak so that the torque reaches the lower values or a valley, afterwards, it enters the smooth and relatively steady period until the maximum speed.

The frictional torque evolutions during the stop stages appear to be a thoroughly opposite process. The torques keep steady or drop smoothly from the level at the maximum speed until about the second half of the stop period, and then they ascend to peak points, following which is the final stage where the torques evolve to zero or somewhere random. Especially, same as the start-up stages, the durations from the peaks to the ends are also all about 1 s.

The torque levels differ among seals, rates and stages. The lightest torque level is attributed to the outer-groove seal, while the smooth-face seal has the heaviest. As shown in the figures, for each seal the rapider the rate is, the lower the torque peak is. In addition, the peaks during the start-up stages are usually significantly higher than that during the stop stages.

3.2. Leakage comparison

Due to the transient test and measurement method, it is difficult to collect considerable amount of leakage water to obtain relatively accurate leakage rate. As such, only the results of the 8 s/kr start-up stages are compared among four seals. As shown in **Fig. 9**, for the inner-groove and smooth-face seals,

the leakages are both zero based on the fact that no drop is detected during 28 s; for the middle-groove seal, although the leakage exists, it is very close to zero (less than 0.01 g/min); for the outer-groove seal, it reaches 0.26 g/min, larger than other seals but still acceptable.

4. Discussion

4.1. Torque peaks

As described in the former section, the torque peaks appear in all evolution curves at almost the same time for the start-up stages or at almost the same remaining time for the stop stages regardless of the seal types and the speed-varying rates. If we divide the torque evolutions of both start-up and stop stages into three segments, for the former they can be Segment I (Seg. I) before peak, Segment II (Seg. II) dropping and Segment III (Seg. III) smooth, while for the latter they can be Seg. I smooth, Seg. II rising and Seg. III after peak. For all 60 curves of the start-up stages shown in **Fig. 5** ~ **Fig. 8**, the Seg. I all lasts about 1 second, while for the rest 60 curves of the stop stages, the Seg. III remains also about 1 second.

This time duration between the start (or stop) and the peak, which could be linked to the measurement technique, is supposed to be a system value rather than a Tribological effect as it is independent of acceleration (or deceleration) and groove types. Therefore, Seg. I of the start-up stage and Seg. III of the stop stage will not be analyzed in this paper.

4.2. Lift-off mechanism of the seals

The frictional torque - rotation speed relationships are presented for four seal types and two stages in **Fig. 10**. Note that all curves in this section are the average of three repeated tests.

Based on the evolution of the torque that decreases with the speed, it is clear that a fluid carrying capacity is developed for each type of seal. According to the fundamental concept of the Stribeck Curve, a “frictional coefficient - duty number relationship” with a valley tendency can represent the transition from the mixed lubrication state to the full-film lubrication regime. In this paper, the frictional torque can represent the frictional coefficient and the rotation speed can represent the duty number, because the other parameters (fluid pressure and viscosity) are all set to identical values in all cases. Accordingly, it could be deduced that the outer-groove and middle-groove seals reach the full-film lubrication, while the inner-groove and smooth-face seals run in the mixed lubrication state.

4.2.1. Hydrodynamic effect

The hydrodynamic effect induced by the herringbone grooves is expected to generate the lift-off

effect and the full-film lubrication regime. It is verified that the torque level increases when the grooves are apart from the pressured fluid side. For example, the outer-groove seal has dramatically smaller torque peaks (see **Fig. 11**) and smaller maximum-speed torques (see **Fig. 12**) comparing with the middle-groove and inner-groove seals, indicating that it can enter the full-film state even at very small speed. Directly connecting the grooves with the pressured water at the outer diameter effectively improves the groove feeding and diminishes the low-pressure areas accompanied with possible cavitation, contributing to building sufficient load-carrying capacity with certain film thickness. The middle-groove seal exhibits evidently larger torque peaks than the outer-groove seal, indicating that it does not enter the full-film lubrication until the speed is larger enough, but a full film can still be built up afterwards.

According to the Newton's law of viscosity, smaller frictional torque of the fluid film represents larger film thickness. As such, to maintain same load-carrying capacity, the film thickness of the middle-groove seal could be smaller. Although the out-groove seal could have larger leakage (see **Fig. 9**), the longer segments of the herringbone grooves can produce the upstream-pumping effect to restrict the leakage to an acceptable level.

As for the inner-groove seal, it has far larger peak torques and larger maximum-speed torques which are close to those of the smooth-face seal (see **Figs. 11 and 12**), meanwhile, the curves cannot reach the slightly ascending period that is regarded as the typical feature of hydrodynamic full film regime. Connecting with the ambient at the inner-diameter side and far from the pressured water, the inner herringbone grooves fail to generate sufficient high-pressure areas in the fluid film.

4.2.2. Hydrostatic effect

Due to the coning induced by the heat generation on the seal faces and thereby the hydrostatic effect, it is possible to reach full-film condition as the seal is balanced [34]. In steady-state condition, the amount of coning is proportional to the power entering the face and is thus proportional to the frictional torque for a given rotational speed. When the efficiency of the groove is decreased, increase in the torque yields more coning and more hydrostatic effect to help to lift off. This is what happens to the inner-groove and smooth-face seals which balance at larger steady torques to make their faces coned enough.

Influence of the acceleration on the torque - speed relationships further approves the function of the hydrostatic effect on the inner-groove and smooth-face seals. Due to the thermal lag effect on the seal rings, it costs a certain time to conduct the heat from the face to the surroundings. Therefore, if the speeding up is rapider, the formation of the face coning will be delayed until larger speed, which also

postpones the better lubrication state resulted from the hydrostatic effect [35].

4.2.3. Squeeze effect

In addition, it can be seen that the squeeze effect is also involved by comparing results of the start-up and stop stages. As shown in **Fig. 13**, except for the outer-groove cases (see **Fig. 13(a1) ~ (a5)**), the curves of the stop stage are always evidently lower than those of the start-up stage when the speed is smaller than certain values. During the start-up stage, the film thickness increases with time as friction decreases, thus squeeze effect creates a negative force. On the opposite, during the stop stage, it decreases with time providing an additional lift-off effect. It allows to reduce the frictional torque peak by limiting asperity contact as it is observed particularly for the middle-groove, inner-groove and smooth-face seals.

As the seals work at thinner film, the squeeze effect that is a function of the film thickness at the power -3 is obviously enhanced. That is why the difference between start-up and stop torque peaks is increased when the grooves are less efficient to generate a full film. This effect is enhanced when there are no grooves.

4.3. Steady state operation

From the maximum-speed torque (M_{3500}) comparison (see **Fig. 12**), two important features can be observed: (i) for all seals and all speed-varying rates, M_{3500} of the start-up stages are equal to those of the stop stages, (ii) for each seal, M_{3500} are same among all speed-varying rates. These features indicate that the steady state have already been reached at the final of the speeding up even for the rapidest acceleration case (the 0.5 s/kr case) for all seals. The thermal characteristic time due to the thermal lag effect is smaller than the acceleration (or deceleration) duration.

Accordingly, it can be further approved that the squeeze effect plays an irreplaceable role on the seals' transient processes, because the difference between the start-up and stop stages is still considerable even for lower speed-varying rates when the thermal balance can be reached on time. However, for the 0.5 s/kr case, the thermal lag effect probably has an effect on to the difference between the start-up and stop curves more or less.

5. Conclusions

The transient frictional-torque variations of mechanical face seals during start-up and stop stages are experimentally measured. The outer-diameter-side, middle and inner-diameter-side herringbone-grooved face seals and a smooth-face seal are tested. Tests are executed on a formerly developed test rig with a

dedicated mechanism for the direct measurement of the face-seal frictional torque. The fluid film development and generation of four seals during the transient processes are deduced according to the torque evolutions, and thereby the lift-off mechanisms of the seals are analyzed and discussed.

The hydrodynamic effect of the herringbone grooves diminishes as the grooved area gets apart from the pressured fluid side. Full film can build up at very small rotation speed for the outer-groove seal and at a larger speed for the middle-groove seal. The inner-groove seal fails to yield evident hydrodynamic effect so that it performs similarly with the smooth-face seal.

The hydrostatic effect dominates the fluid film formation when the grooves function inadequately. More heat generation on the seal faces produces more face coning and thereby more sufficient hydrostatic effect to develop the fluid film. The frictional torques of the inner-groove and smooth-face seals keeps decreasing from large values until it reaches a balanced state among the “lubrication - heat generation - face coning coupling”. Changing the speed-varying rate has more considerable influence on the development of the hydrostatic effect rather than the hydrodynamic effect, particularly in the start-up stages.

Comparison among the torque values at the maximum speed demonstrates that the thermal characteristic time of the seal is smaller than even the shortest acceleration duration (the 0.5 s/kr case). Therefore, the squeezed effect is responsible for the phenomenon allowing the stop processes to experience evidently lower frictional torque than the start-up stages.

CRediT authorship contribution statement

Yongfan Li: Conceptualization, Data curation, Formal analysis, Funding acquisition, Investigation, Methodology, Validation, Visualization, Writing - Original Draft, Writing - Review & Editing. **Noël Brunetière:** Conceptualization, Data curation, Formal analysis, Funding acquisition, Investigation, Methodology, Project administration, Resources, Software, Supervision, Writing - Review & Editing. **Muming Hao:** Conceptualization, Funding acquisition, Methodology, Project administration, Resources, Supervision, Writing - Review & Editing. **Tianzhao Li:** Visualization. **Fuyu Liu:** Visualization.

Declaration of Competing Interest

The authors declare that they have no known competing financial interests or personal relationships that could have appeared to influence the work reported in this paper.

Acknowledgements

This work has been supported by the National Natural Science Foundation of China (Grant number 51975585) and the China Scholarship Council (Grant number 201906450039). This work also pertains to the French government program Investissements Avenir (LABEX INTERACTIFS, reference ANR-11-LABX-0017-01, and EUR INTREE, reference ANR-18-EURE-0010).

References

[1] Lebeck A O. Principles and design of mechanical face seals[M]. John Wiley & Sons, 1992.

[2] Li Z, Li Y, Cao H, et al. Investigation of cavitation evolution and hydrodynamic performances of oil film seal with spiral groove[J]. Tribology International, 2021, 157: 106915.

[3] Li Z, Hao M, Sun X, et al. Experimental study of cavitation characteristic of single-row reverse spiral groove liquid-film seals[J]. Tribology International, 2020, 141: 105782.

[4] Li Y, Hao M, Sun X, et al. Dynamic response of spiral groove liquid film seal to impact conditions[J]. Tribology International, 2020, 141: 105865.

[5] Zhang G, Chen G, Zhao W, et al. An experimental test on a cryogenic high-speed hydrodynamic non-contact mechanical seal[J]. Tribology letters, 2017, 65(3): 1-11.

[6] Rouillon M, Brunetière N. Spiral groove face seal behavior and performance in liquid lubricated applications[J]. Tribology Transactions, 2018, 61(6): 1048-1056.

[7] Zhang G Y, Zhao W G, Yan X T, et al. A theoretical and experimental study on characteristics of water-lubricated double spiral–grooved seals[J]. Tribology Transactions, 2011, 54(3): 362-369.

[8] Lai W T. Face seal with double spiral grooves: U.S. Patent 5,201,531[P]. 1993-4-13.

[9] Meng X, Zhao W, Shen M, et al. Thermohydrodynamic analysis on herringbone-grooved mechanical face seals with a quasi-3D model[J]. Proceedings of the Institution of Mechanical Engineers, Part J: Journal of Engineering Tribology, 2018, 232(11): 1402-1414.

[10] Strom T N, Ludwig L P, Allen G P, Johnson R L. Spiral groove face seal concepts; comparison to conventional face contact seals in sealing liquid sodium (400 to 1000 Deg F)[J]. ASME Journal of Lubrication Technology, 1968, 90(2): 450-462.

[11] Wang Y. Face seal with spiral grooves: U.S. Patent 6,152,452[P]. 2000-11-28.

[12] Wang Y, Wang J, Yang H, et al. Theoretical analyses and design guidelines of oil-film-lubricated mechanical face seals with spiral grooves[J]. Tribology Transactions, 2004, 47(4): 537-542.

[13] Wang Y, Yang H, Wang Y, et al. Experimental investigations and field applications of oil-film-lubricated mechanical face seals with spiral grooves[J]. Tribology transactions, 2005, 48(4): 589-596.

[14] Zhang G, Zhao Y, Zhao W, et al. An experimental study on the cryogenic face seal at different inlet pressures[J]. Proceedings of the Institution of Mechanical Engineers, Part J: Journal of Engineering Tribology, 2020, 234(9): 1470-1481.

[15] Zheng X, Gardner J, Berard G. Adaptive divert double-spiral groove face seals for high speed, high temperature applications[C]//36th AIAA/ASME/SAE/ASEE Joint Propulsion Conference and Exhibit. 2000: 3373.

[16] Zheng X, Berard G. Development of non-contacting, film-riding face seals for large-diameter gas engines[C]//37th Joint Propulsion Conference and Exhibit. 2001: 3624.

[17] Berard G, Zheng X. Analysis and design of a double-divert spiral groove seal[C]//42nd AIAA/ASME/SAE/ASEE Joint Propulsion Conference & Exhibit. 2006: 4753.

[18] Xu L, Wu J H, Wang Y, et al. A novel compound mechanical seal of reusable rocket turbopump with superconducting magnetic force improving lubrication and stability[J]. Tribology International, 2021, 159: 106989.

[19] Chen T, Ji J, Fu Y, et al. Tribological performance of UV picosecond laser multi-scale composite textures for C/SiC mechanical seals: Theoretical analysis and experimental verification[J]. Ceramics International, 2021, 47(16): 23162-23180.

[20] Chang X, Teng W, Zhang P, et al. Experimental Verification on Friction Factor Fractal Model of the End Faces for Mechanical Seals[C]//IOP Conference Series: Materials Science and Engineering. IOP Publishing, 2019, 493(1): 012150.

[21] Adjemout M, Brunetière N, Bouyer J. Friction and temperature reduction in a mechanical face seal by a surface texturing: comparison between TEHD simulations and experiments[J]. Tribology Transactions, 2018, 61(6): 1084-1093.

[22] Ayadi K, Brunetière N, Tournerie B, et al. Experimental and numerical study of the lubrication regimes of a liquid mechanical seal[J]. Tribology International, 2015, 92: 96-108.

[23] Ayadi K, Brunetiere N, Tournerie B, et al. Experimental thermal analysis of a mechanical face seal[J]. Journal of Thermal Science and Engineering Applications, 2016, 8(3): 031011.

[24] Xue B, Wei C, Hu J B, et al. Numerical and experimental study on the separation characteristics of microgroove rotary seals[J]. Proceedings of the Institution of Mechanical Engineers, Part D: Journal

of Automobile Engineering, 2017, 231(7): 963-972.

[25] Zhao Y, Wei C, Yuan S, et al. Theoretical and experimental study of cavitation effects on the dynamic characteristic of spiral-groove rotary seals (SGRSs)[J]. Tribology letters, 2016, 64(3): 1-18.

[26] Hu J B, Wei C, Li X Y. Experimental investigation on the friction and sealing characteristics of narrow end-face seal ring with spiral grooves for wet clutch[J]. Industrial Lubrication and Tribology, 2015.

[27] Ma C, Gu W, Tu Q, et al. Experimental investigation on frictional property of mechanical seals with varying dimple diameter along the radial face[J]. Advances in Mechanical Engineering, 2016, 8(8): 1687814016664837.

[28] Xu J, Peng X, Bai S, et al. Experiment on wear behavior of high pressure gas seal faces[J]. Chinese Journal of Mechanical Engineering, 2014, 27(6): 1287-1293.

[29] Ding X, Lu J. Theoretical analysis and experiment on gas film temperature in a spiral groove dry gas seal under high speed and pressure[J]. International Journal of Heat and Mass Transfer, 2016, 96: 438-450.

[30] Feng X, Su W, Ma Y, et al. Numerical and experimental study on waviness mechanical seal of reactor coolant pump[J]. Processes, 2020, 8(12): 1611.

[31] Wang T, Huang W, Liu X, et al. Experimental study of two-phase mechanical face seals with laser surface texturing[J]. Tribology International, 2014, 72: 90-97.

[32] Qiu Y, Khonsari M M. Experimental investigation of tribological performance of laser textured stainless steel rings[J]. Tribology International, 2011, 44(5): 635-644.

[33] Chen Y, Peng X, Jiang J, et al. Experimental and theoretical studies of the dynamic behavior of a spiral-groove dry gas seal at high-speeds[J]. Tribology International, 2018, 125: 17-26.

[34] Brunetiere N. An analytical approach of the thermoelastohydrodynamic behaviour of mechanical face seals operating in mixed lubrication[J]. Proceedings of the Institution of Mechanical Engineers, Part J: Journal of Engineering Tribology, 2010, 224(12): 1221-1233.

[35] Green I. A transient dynamic analysis of mechanical seals including asperity contact and face deformation[J]. Tribology transactions, 2002, 45(3): 284-293.

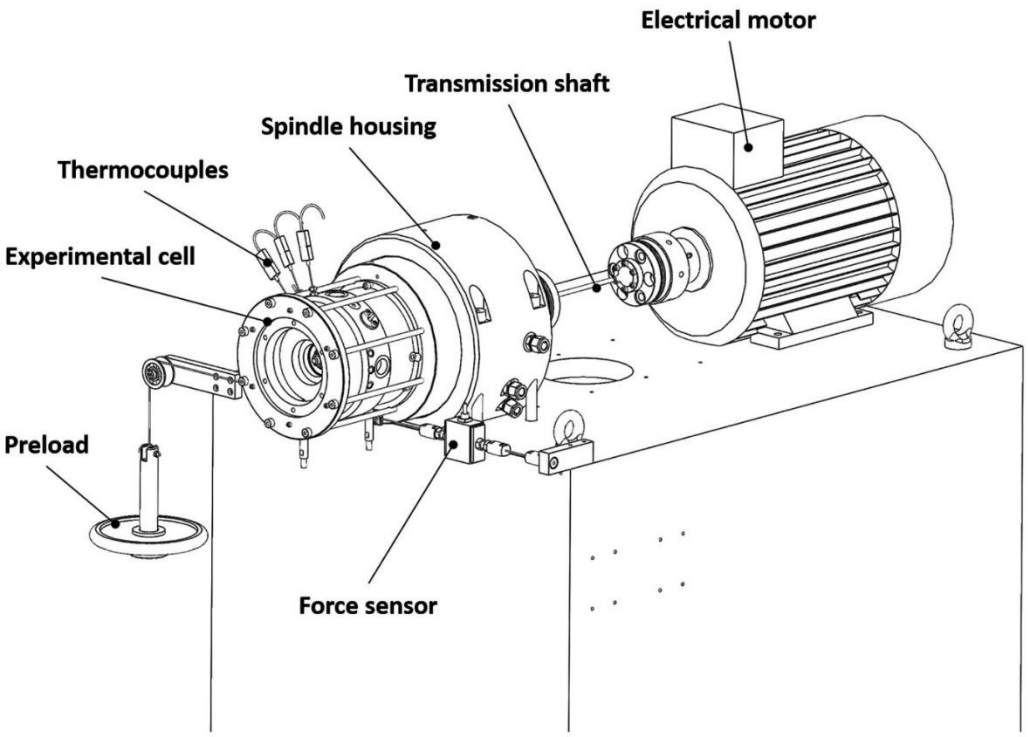

(a)

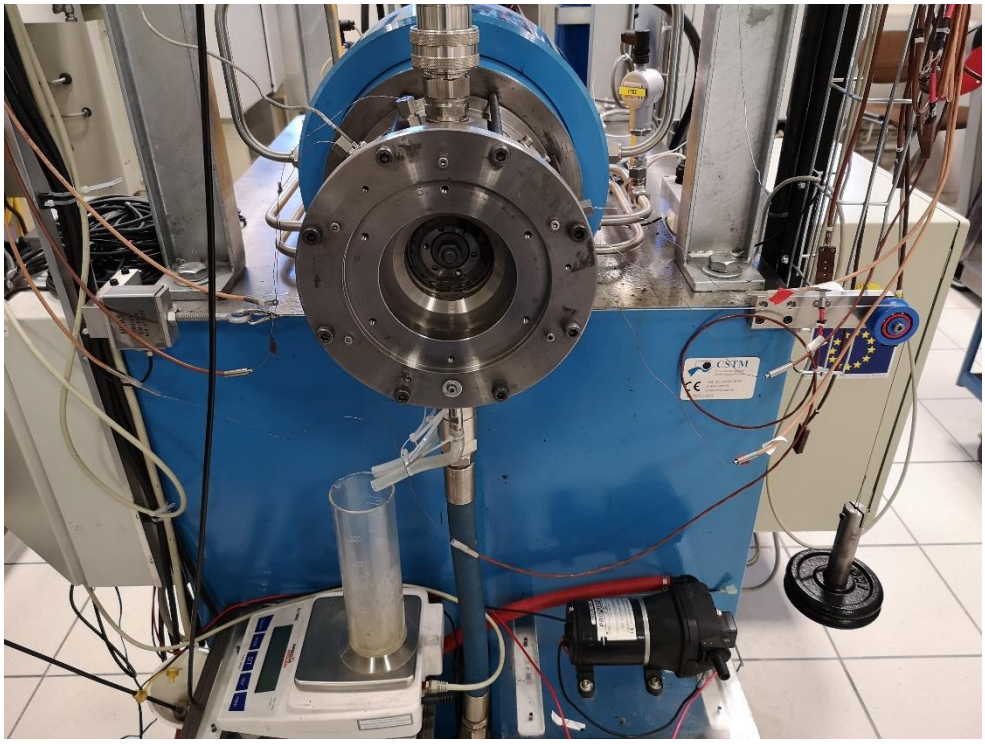

(b)

Fig. 1. The test rig: (a) the general view [6], (b) photo from the front.

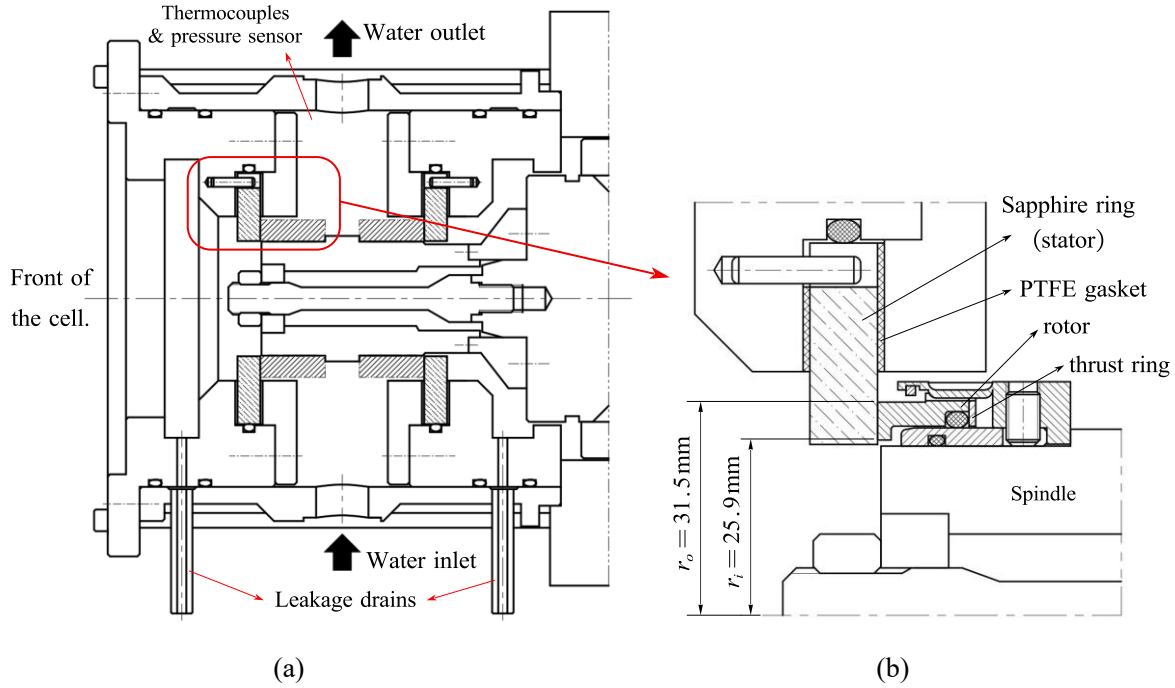

Fig. 2. Cross-section structure: (a) experimental cell, (b) mechanical face seal.

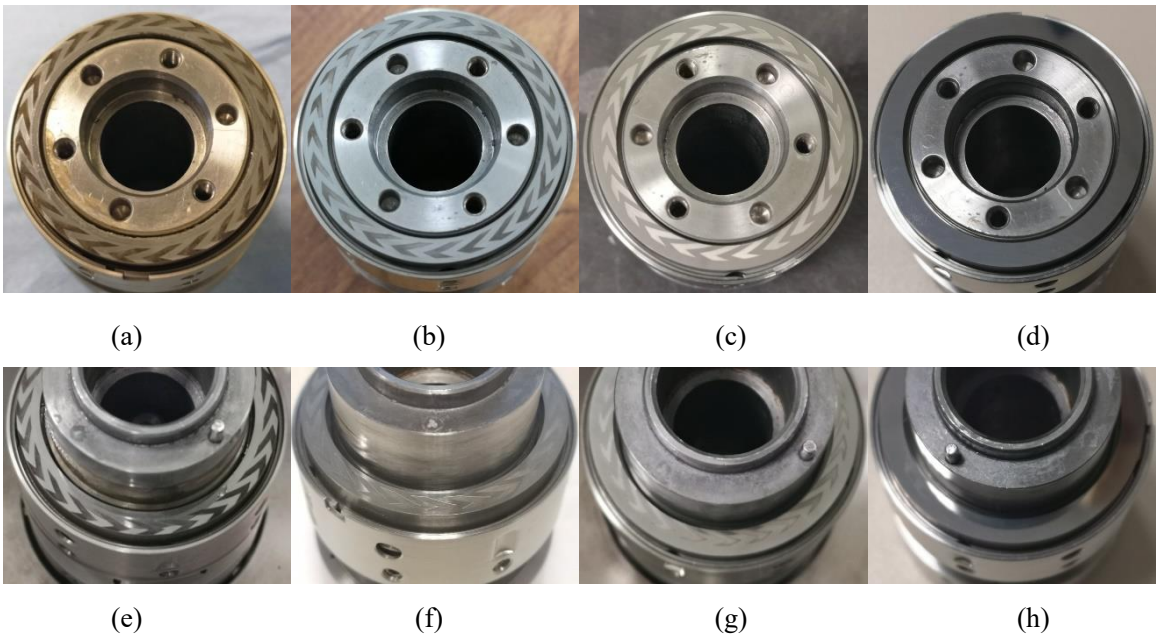

(a) (b) (c) (d)

(e) (f) (g) (h)

Fig. 3. Tested rotating assembly and the rotor faces: (a) front-side, outer-groove, (b) front-side, middle-groove, (c) front-side, inner-groove, (d) front-side, smooth-face, (e) back-side, outer-groove, (f) back-side, middle-groove, (g) back-side, inner-groove, (h) back-side, smooth-face.

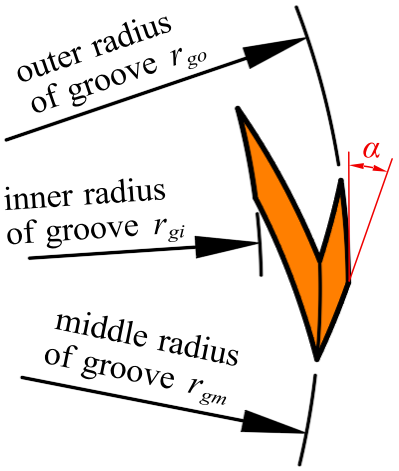

Fig. 4. Geometry and structural parameters of one single herringbone groove.

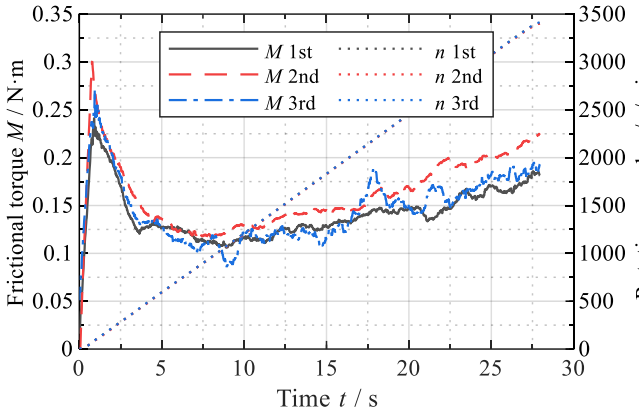

(a1)

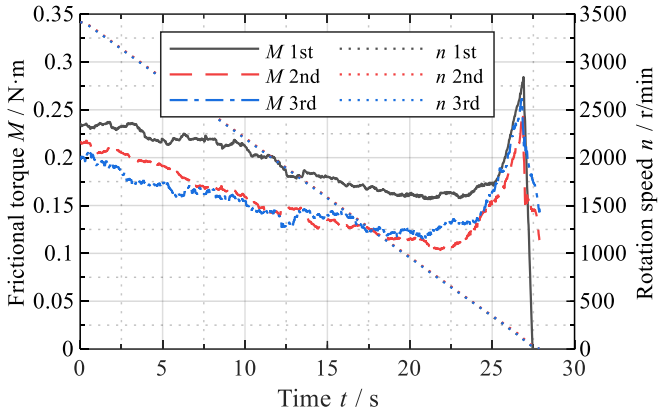

(a2)

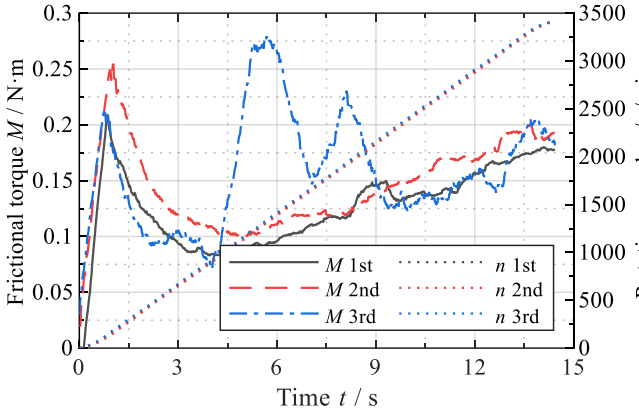

(b1)

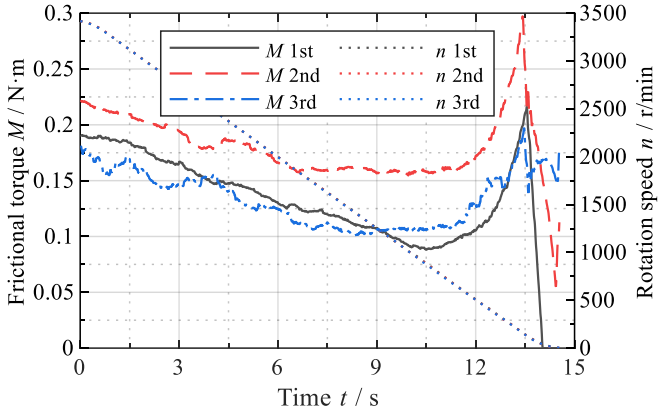

(b2)

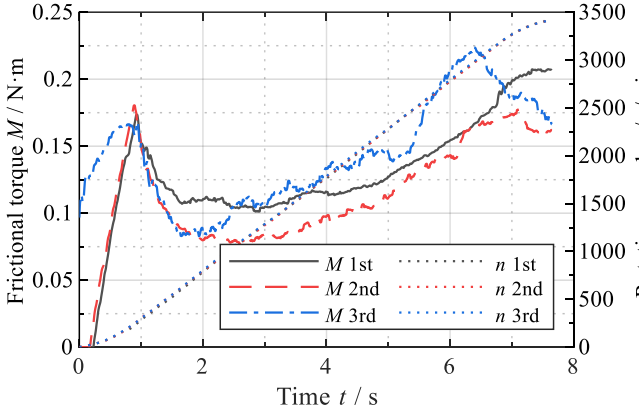

(c1)

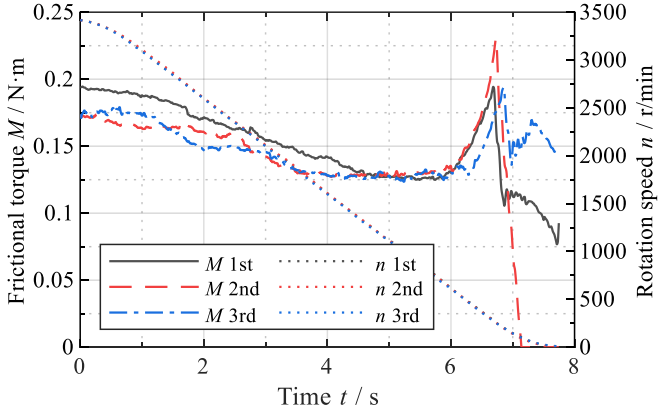

(c2)

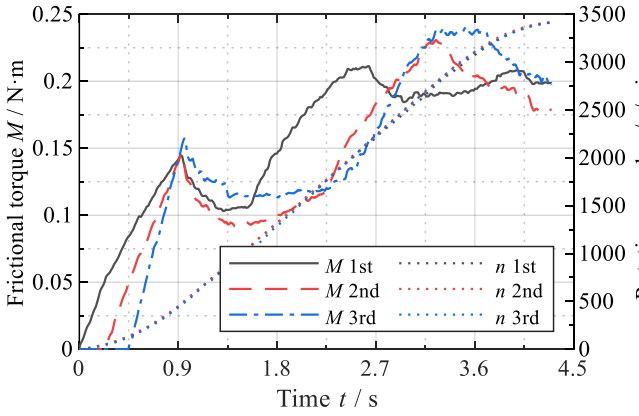

(d1)

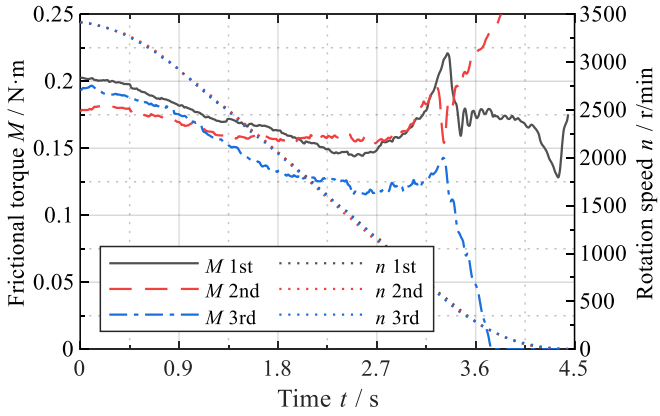

(d2)

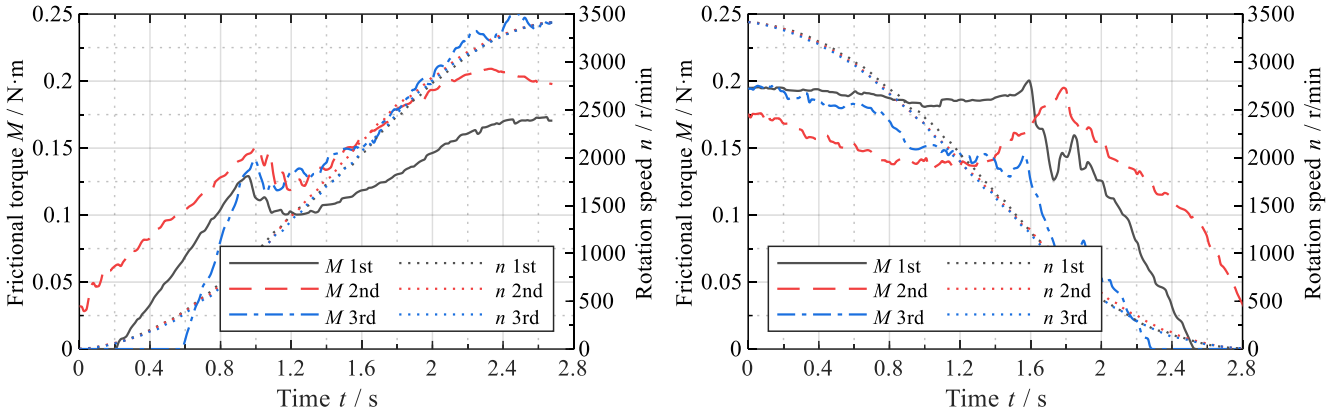

Fig. 5. Original data of the frictional torque evolutions - outer-groove seal:

(a1) 8 s/kr, start-up, (a2) 8 s/kr, stop,

(b1) 4 s/kr, start-up, (b2) 4 s/kr, stop,

(c1) 2 s/kr, start-up, (c2) 2 s/kr, stop,

(d1) 1 s/kr, start-up, (d2) 1 s/kr, stop,

(e1) 0.5 s/kr, start-up, (e2) 0.5 s/kr, stop.

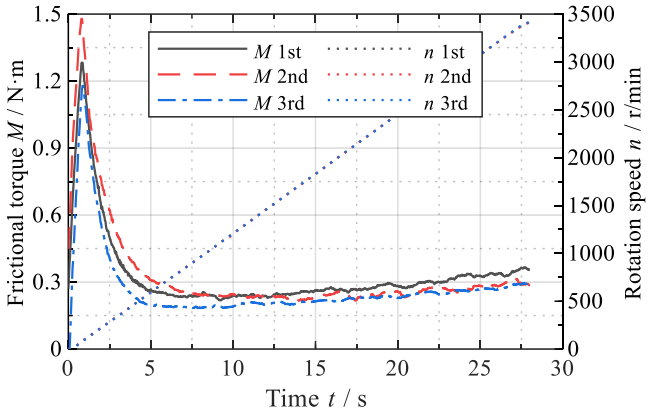

(a1)

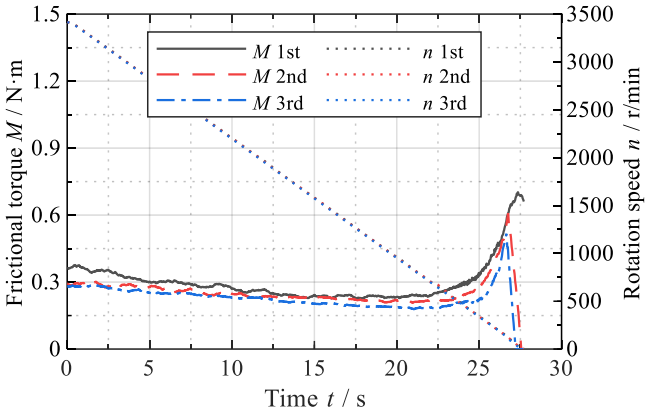

(a2)

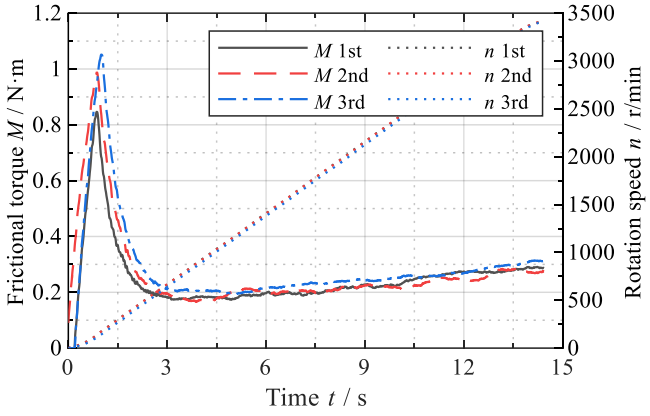

(b1)

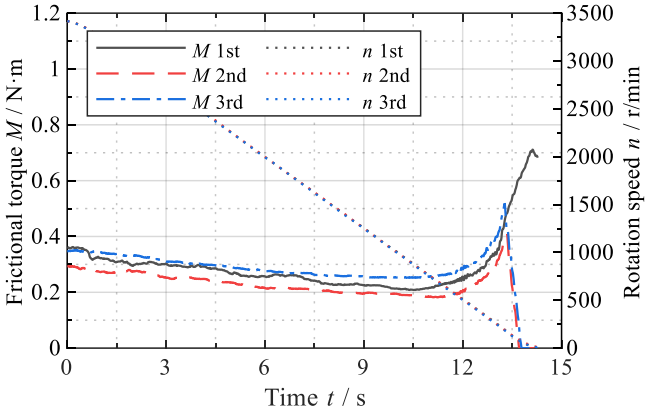

(b2)

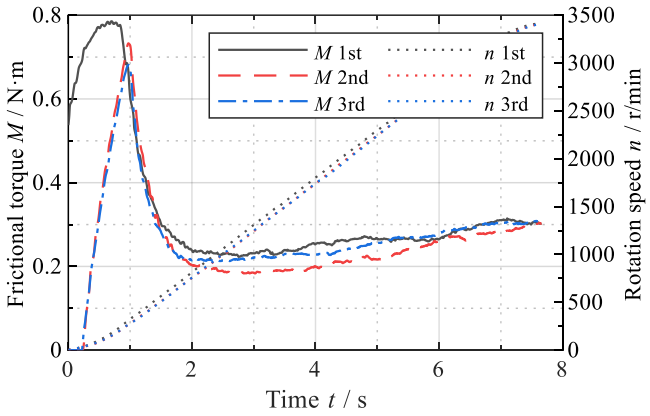

(c1)

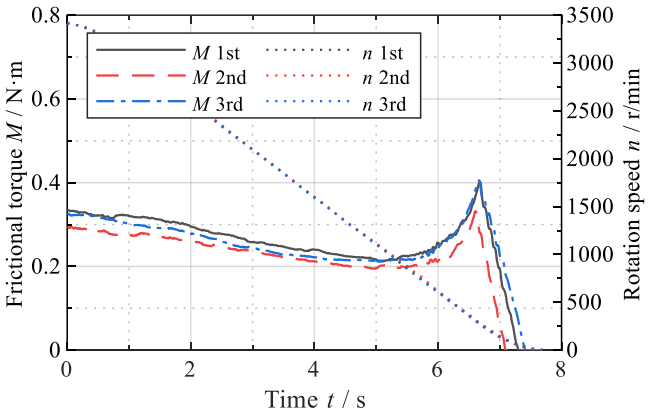

(c2)

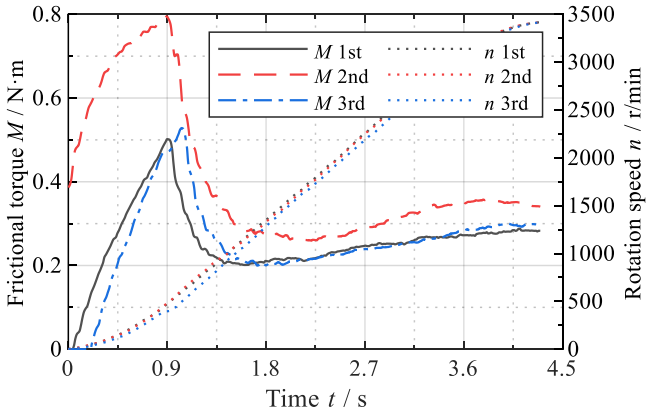

(d1)

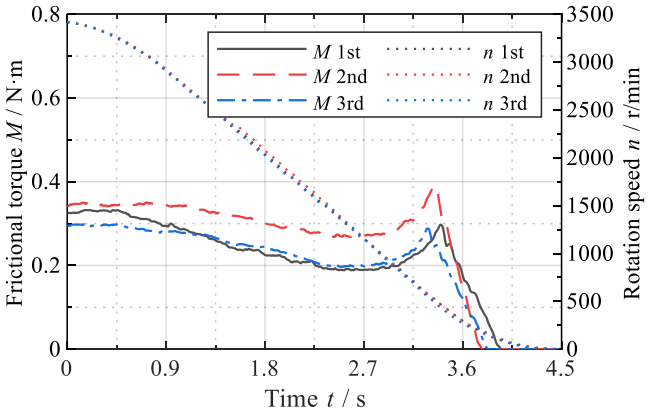

(d2)

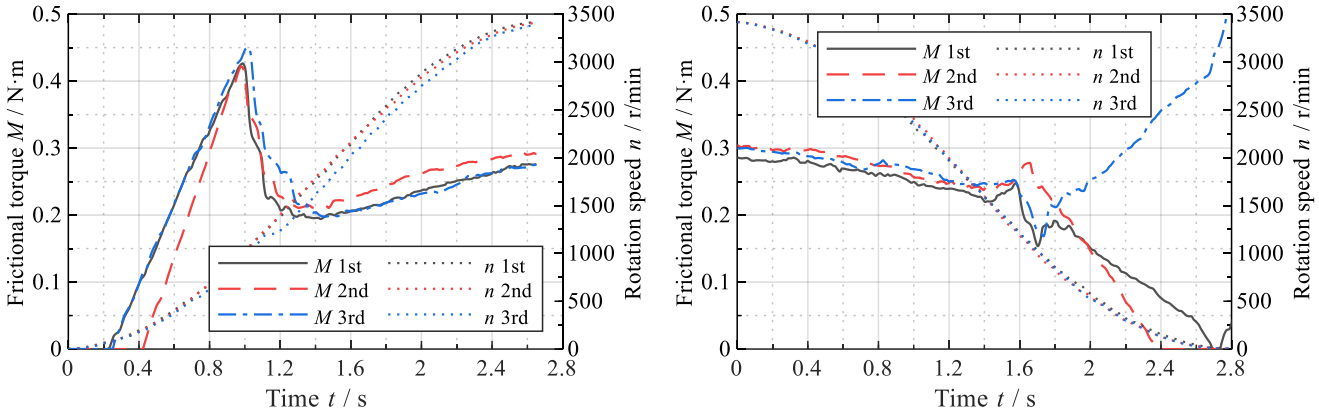

Fig. 6. Original data of the frictional torque evolutions - middle-groove seal:

(a1) 8 s/kr, start-up, (a2) 8 s/kr, stop,

(b1) 4 s/kr, start-up, (b2) 4 s/kr, stop,

(c1) 2 s/kr, start-up, (c2) 2 s/kr, stop,

(d1) 1 s/kr, start-up, (d2) 1 s/kr, stop,

(e1) 0.5 s/kr, start-up, (e2) 0.5 s/kr, stop.

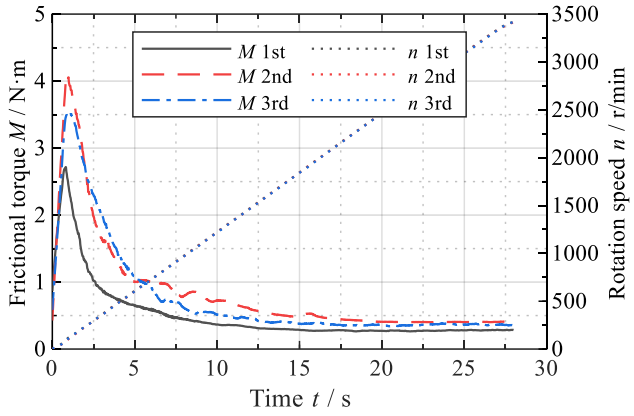

(a1)

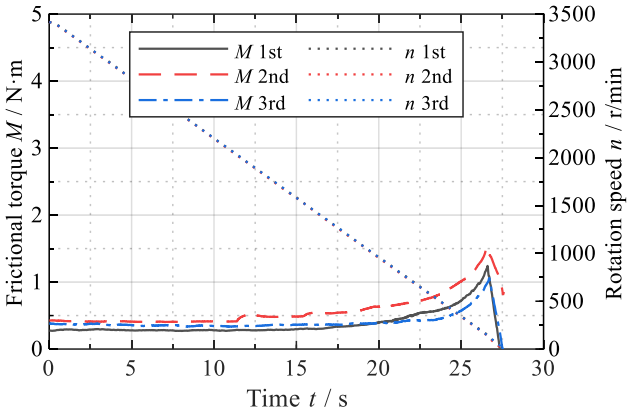

(a2)

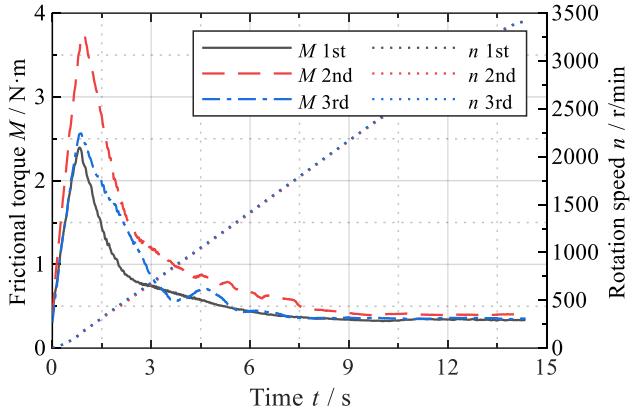

(b1)

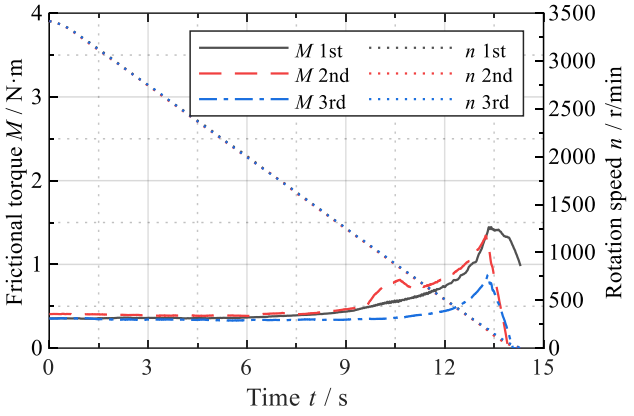

(b2)

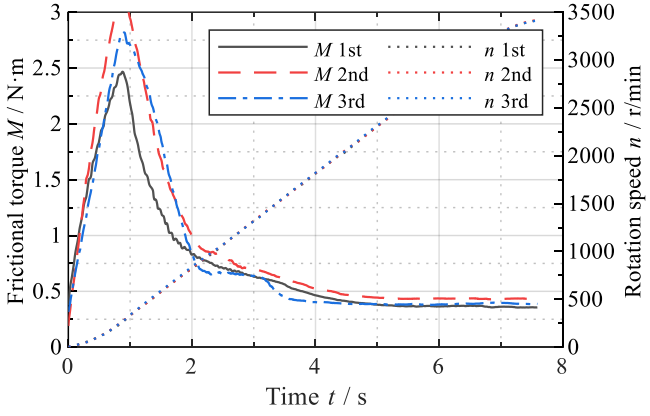

(c1)

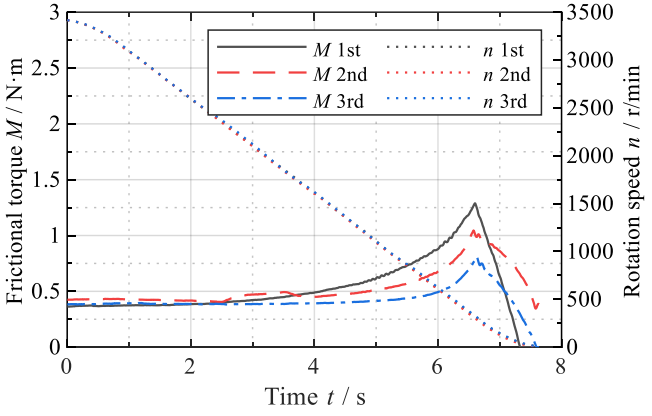

(c2)

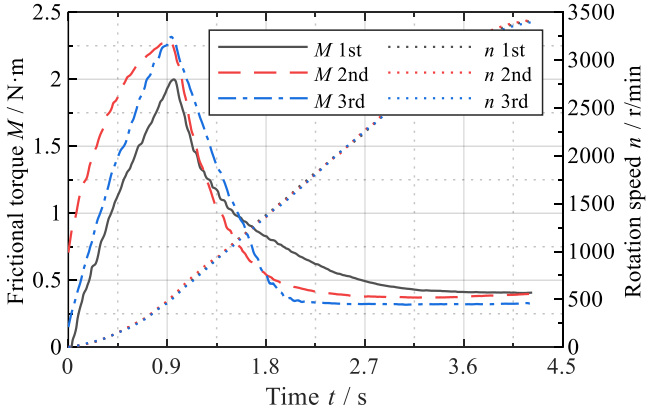

(d1)

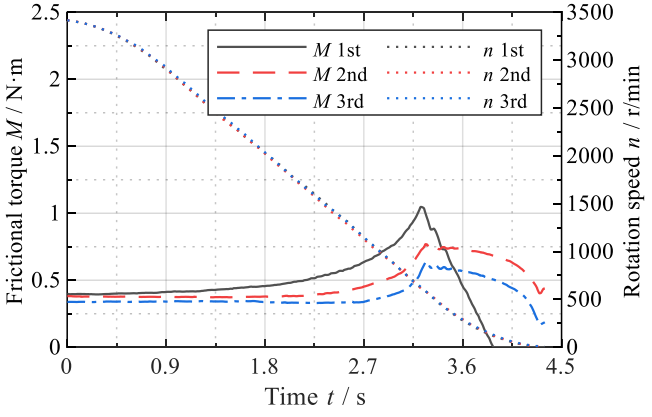

(d2)

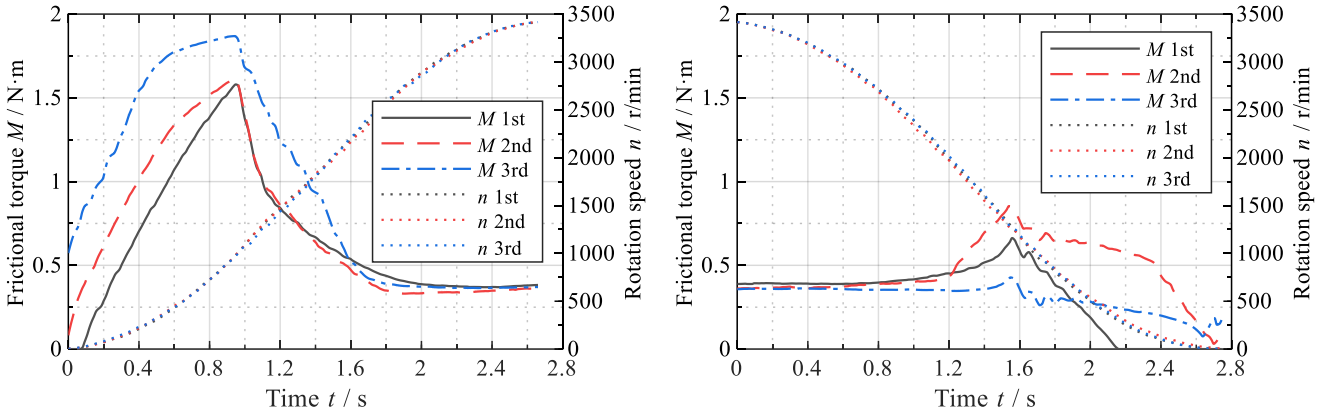

Fig. 7. Original data of the frictional torque evolutions - inner-groove seal:

(a1) 8 s/kr, start-up, (a2) 8 s/kr, stop,

(b1) 4 s/kr, start-up, (b2) 4 s/kr, stop,

(c1) 2 s/kr, start-up, (c2) 2 s/kr, stop,

(d1) 1 s/kr, start-up, (d2) 1 s/kr, stop,

(e1) 0.5 s/kr, start-up, (e2) 0.5 s/kr, stop.

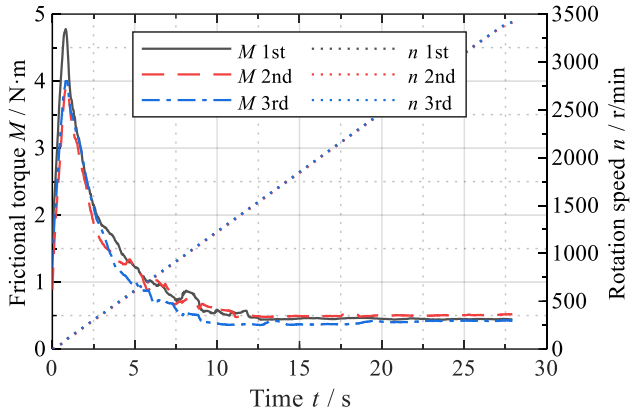

(a1)

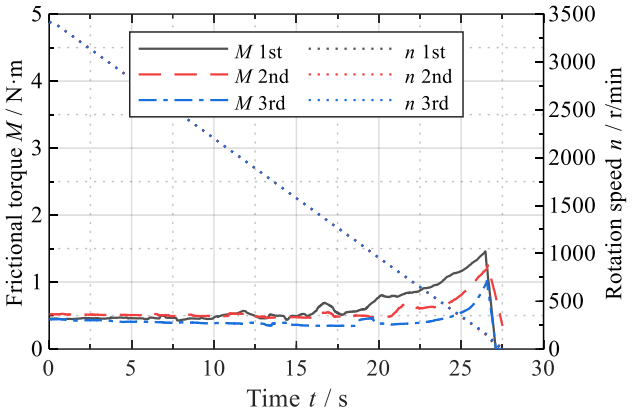

(a2)

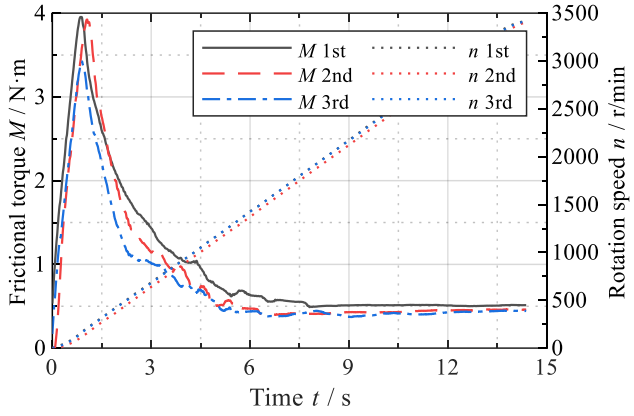

(b1)

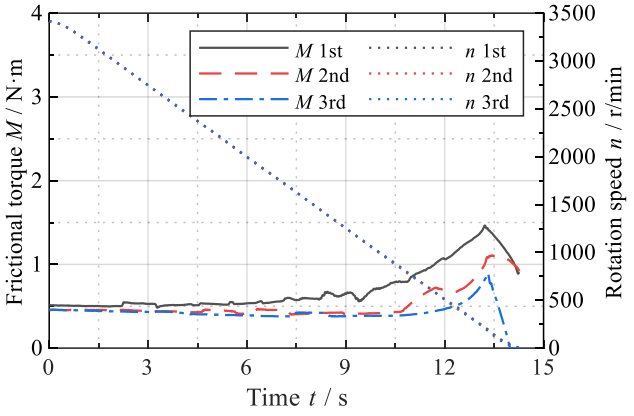

(b2)

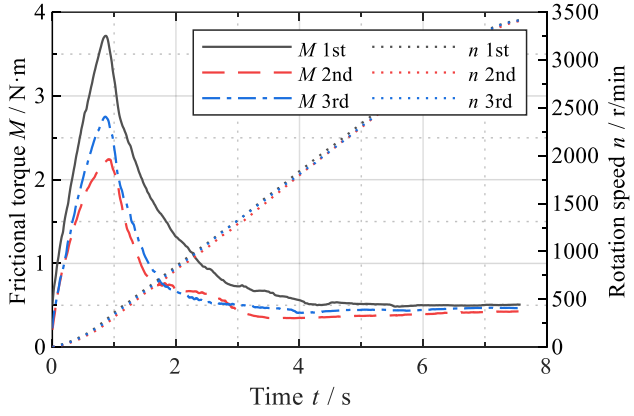

(c1)

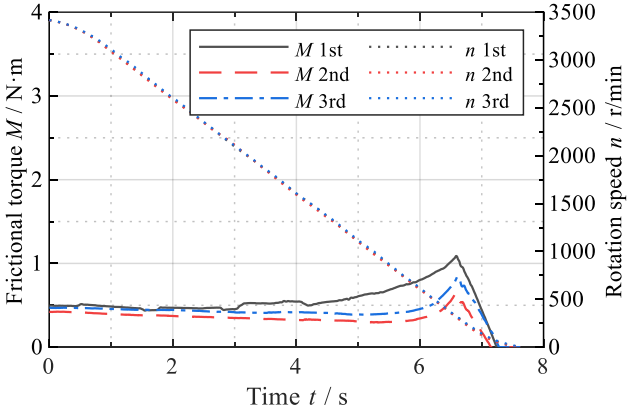

(c2)

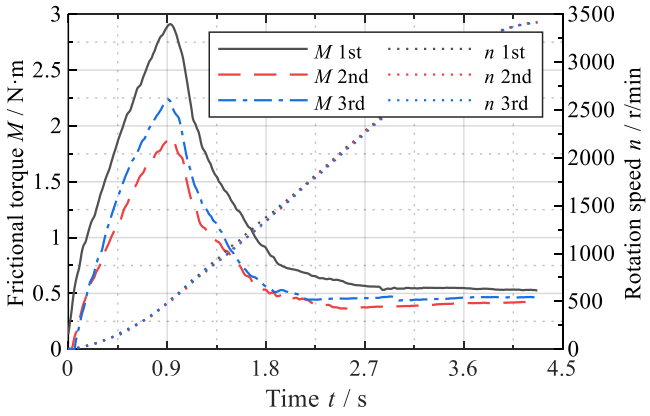

(d1)

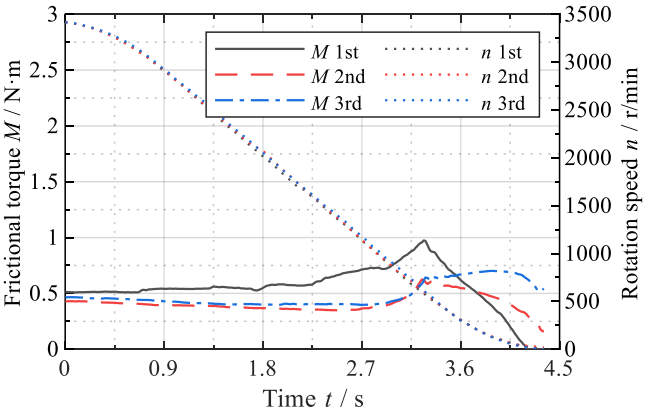

(d2)

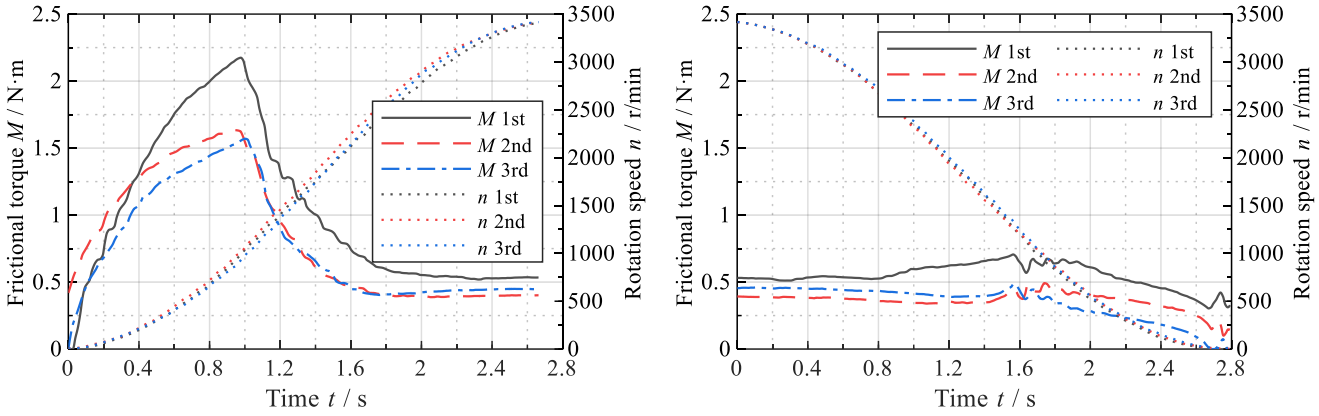

Fig. 8. Original data of the frictional torque evolutions - smooth-face seal:

(a1) 8 s/kr, start-up, (a2) 8 s/kr, stop,

(b1) 4 s/kr, start-up, (b2) 4 s/kr, stop,

(c1) 2 s/kr, start-up, (c2) 2 s/kr, stop,

(d1) 1 s/kr, start-up, (d2) 1 s/kr, stop,

(e1) 0.5 s/kr, start-up, (e2) 0.5 s/kr, stop.

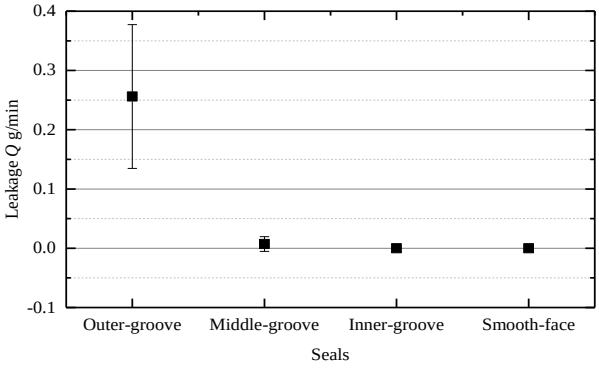

Fig. 9. Leakages of the 8 s/kr start-up cases.

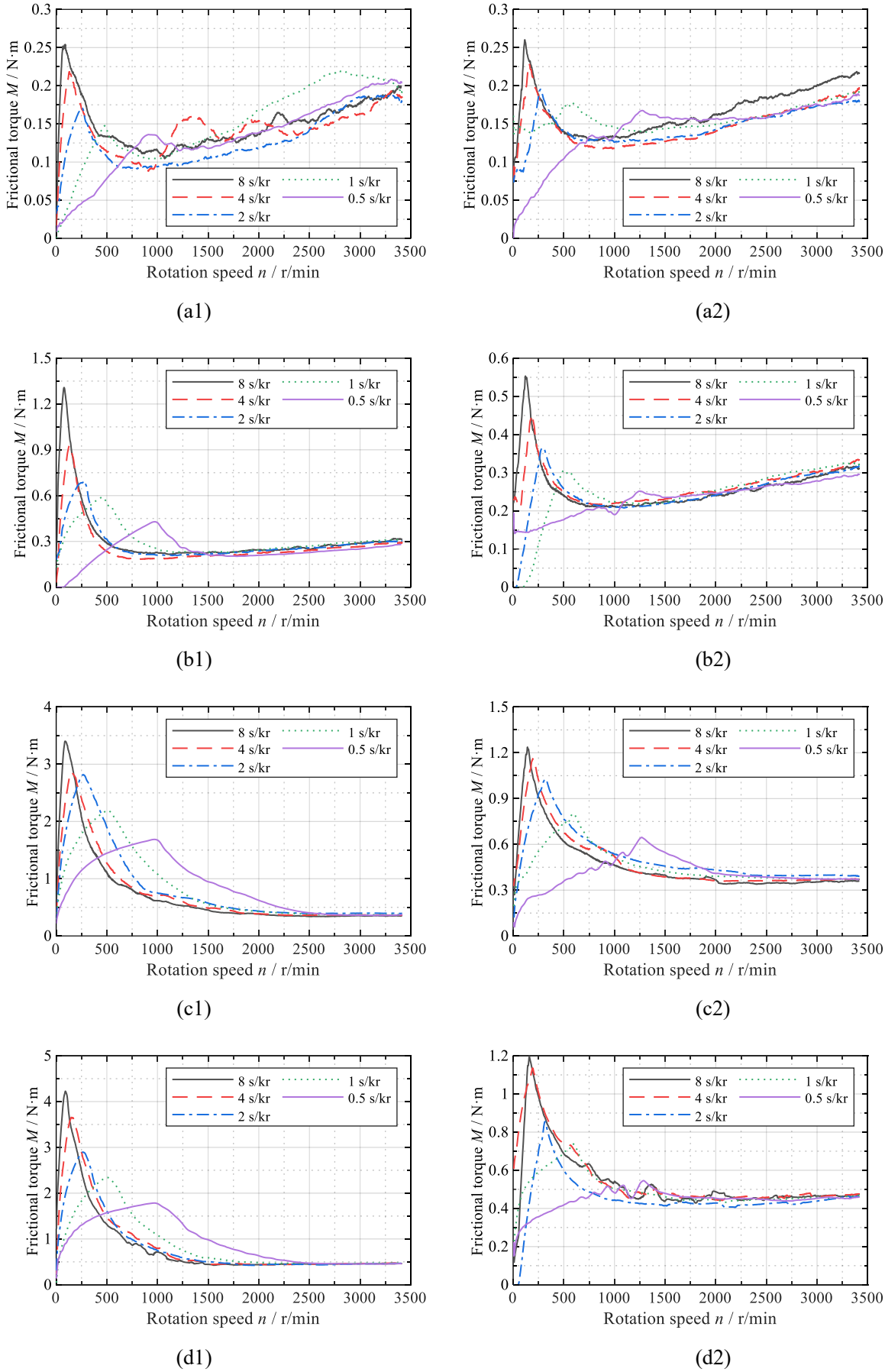

Fig. 10. Frictional torque - rotation speed relationships: (a1) outer-groove seal, start-up, (a2) outer-groove seal, stop, (b1) middle-groove seal, start-up, (b2) middle-groove seal, stop, (c1) inner-groove seal, start-up, (c2) inner-groove seal, stop, (d1) smooth-face seal, start-up, (d2) smooth-face seal, stop.

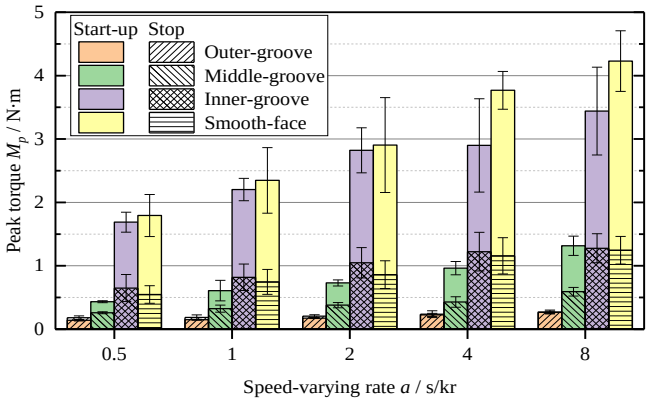

Fig. 11. The peaks of the frictional torque evolution curves.

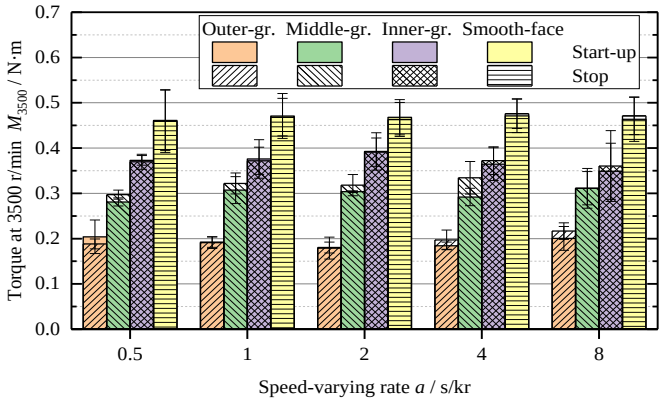

Fig. 12. The frictional torques at the maximum speed (3500 r/min).

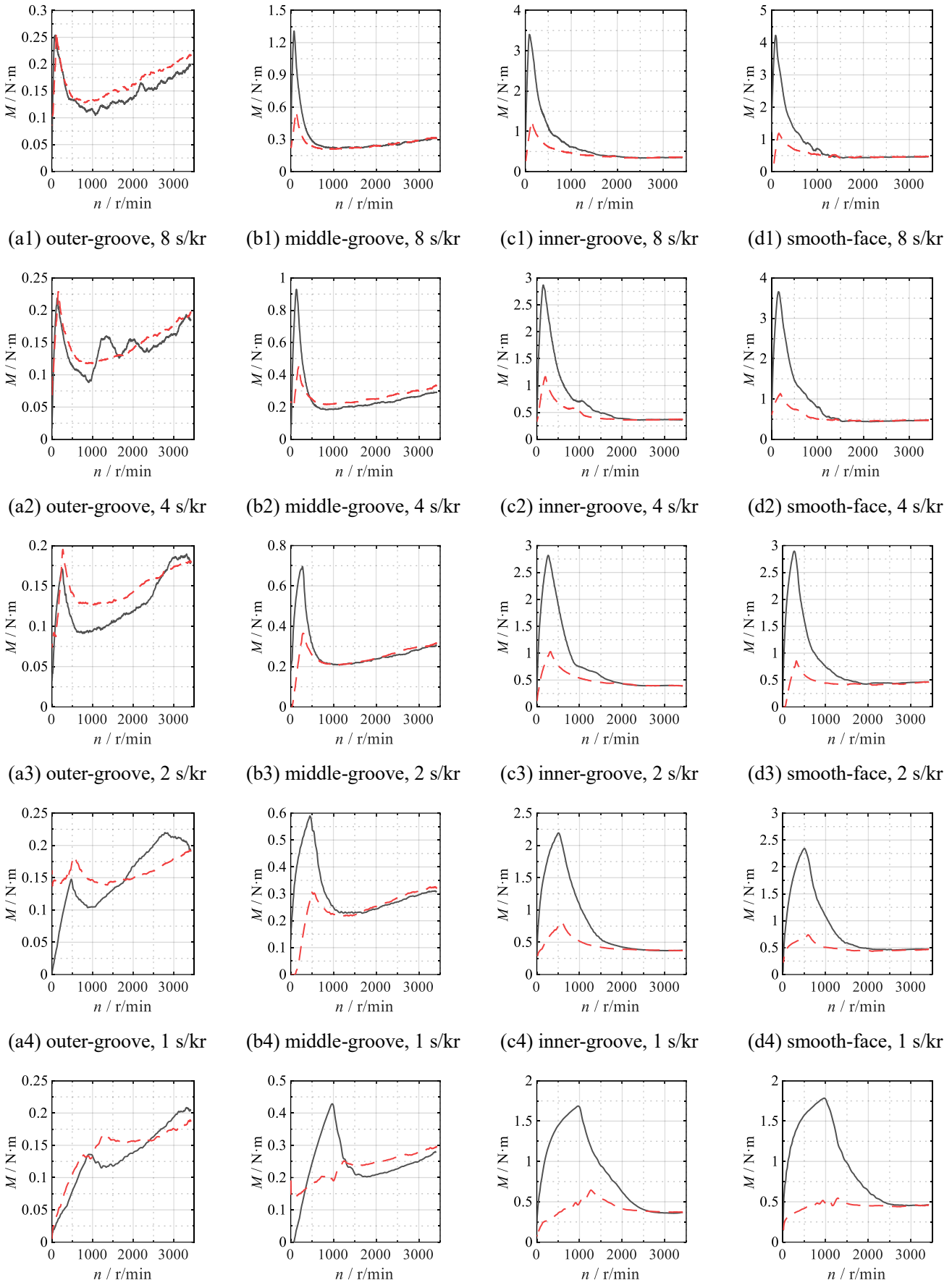

(a1) outer-groove, 8 s/kr (b1) middle-groove, 8 s/kr (c1) inner-groove, 8 s/kr (d1) smooth-face, 8 s/kr

(a2) outer-groove, 4 s/kr (b2) middle-groove, 4 s/kr (c2) inner-groove, 4 s/kr (d2) smooth-face, 4 s/kr

(a3) outer-groove, 2 s/kr (b3) middle-groove, 2 s/kr (c3) inner-groove, 2 s/kr (d3) smooth-face, 2 s/kr

(a4) outer-groove, 1 s/kr (b4) middle-groove, 1 s/kr (c4) inner-groove, 1 s/kr (d4) smooth-face, 1 s/kr

(a5) outer-groove, 0.5 s/kr (b5) middle-groove, 0.5s/kr (c5) inner-groove, 0.5 s/kr (d5) smooth-face, 0.5 s/kr

Fig. 13. Comparison of the frictional torque - rotation speed relationships between the start-up and stop stages (black solid line for the start-up stage, red dashed line for the stop stage).